Generalized Thue-Morse chains and their physical properties

M. Kolář* and M. K. Ali

Department of Physics, University of Lethbridge, Lethbridge, Canada T1K 3M4

Franco Nori

Physics Department, The University of Michigan, Ann Arbor, Michigan 48109-1120

We study the physical properties of the Thue-Morse chain and its generalizations. After a preliminary discussion of its basic features (e.g., structure factor, location, and relative magnitude of spectral gaps), we focus on (1) the trace maps of generalized Thue-Morse lattices, (2) a detailed analysis of the attractor of the associated dynamical system, (3) the electronic spectra through the trace-map approach, (4) spin excitations in a quantum Ising model in a transverse magnetic field, (5) light transmission through a multilayer, and (6) the diamagnetic properties of Thue-Morse superconducting wire networks and Josephson-junction arrays.

I. INTRODUCTION

The pioneering work of Merlin et al.[1] on aperiodic Fibonacci GaAs-AlAs superlattices has generated a large amount of research activity. The study of the scaling properties of the excitation spectra (electronic spectrum and magnetic excitations) of a Thue-Morse (TM) chain is motivated by the fact that this deterministic structure is more "disordered" than the quasiperiodic (QP) one. In other words, this system has a degree of aperiodicity intermediate between that of QP and random systems. More precisely, the Fourier amplitude spectrum of the TM sequence is *singular continuous*, while that of a QP lattice is one with δ-function peaks (not arranged periodically) and possibly a singular continuous spectrum.

The first experimental realization of a TM GaAs-AlAs superlattice is due to Merlin et al.[2] Other recent works include entropy considerations for the TM sequence,[3] a chain with springs,[4,5] acoustic-phonon transmission,[6] a quantum Ising spin system in a transverse magnetic field,[7] a tight-binding model,[8-10] and the scaling of the peaks of the structure factor.[9,10] We believe that there exist many other structures, such as some of the generalized Fibonacci lattices,[11,12] with properties intermediate between quasiperiodic and random. Tracy[13] also observed such intermediate behavior in the thermodynamic properties of some aperiodic Ising models. It is interesting to note that, with regard to the presence of magnetic phase transition, the quantum TM Ising model behaves as a QP sequence.[14] Also the results of Ref. 8 suggest that the electronic spectra of the TM lattice are intermediate between those of the periodic and QP lattices. This apparent contradiction of some thermodynamic and spectral properties with the results for the structure factor is one of the reasons why a more detailed investigation of lattices of this type is important.

II. THE THUE-MORSE CHAIN

The TM sequence of order N has $M = 2^N$ elements composed of two symbols, 0 and 1, defined recursively as follows:

$$\epsilon_0 = 0 \,, \quad \epsilon_{2n} = \epsilon_n \,, \quad \epsilon_{2n+1} = 1 - \epsilon_n \,. \tag{1}$$

The above equations generate an infinite string of digits that never repeats itself. In spite of this aperiodicity, the TM sequence is *self-similar*.

The Fibonacci and Thue-Morse sequences are both generated by extremely simple substitutions: $0 \rightarrow 1$, $1 \rightarrow 10$ (Fibonacci) and $0 \rightarrow 01$, $1 \rightarrow 10$ (Thue-Morse). The former has been recently studied by many authors in the physics literature (see, for example, Refs. 15-17). However, the latter is relatively unknown to most physicists. Therefore, some background information might be necessary and appropriate.

Sequences generated by substitutions have been studied in several areas of mathematics, computer science, cryptography, and, more recently, physics. One of the first systematic studies of aperiodic sequences was made by Thue[18] in 1906. His results have been rediscovered many times since then. In most cases, these "new" rediscoveries have been made in completely different subjects. Morse[19] studied substitution-generated sequences in the context of topological dynamics. Others have analyzed them in such diverse topics as (i) ergodic theory,[20] (ii) automata theory (tag machines, characterization of recognizable sets of numbers),[21] (iii) formal language theory,[22] (iv) solutions to algebraic equations,[23] and (v) combinatorial theory.[24] This multiplicity of rediscoveries has generated at least ten different ways to define the TM sequence. It is easy to prove that they are all equivalent to each other. We will only mention here the simplest

ways to generate it. The definition based on a recurrence relation has been presented in Eq. (1). Alternatively, let α_n be the number of ones in the binary expansion of n. Thus,

$$\epsilon_n = [1 - (-1)^{\alpha_n}]/2 .$$

Yet another definition starts with the sequence of positive integers. After writing them in binary form, we sum the digits of every integer modulo 2 and obtain the TM sequence. On the other hand, the so-called word concatenation approach starts with $W_0 = 0$, and defines $W_{n+1} = W_n W'_n$ where W'_n is obtained from W_n by exchanging 0 and 1. Thus, $W_1 = 01$, $W_2 = 0110$, $W_3 = 01101001$, $W_4 = 0110100110010110$, and so on. Decimating every other digit in the last sequence, we obtain in the following: decimated $(W_4) = 01101001 = W_3$. In other words, the infinite sequence is not only aperiodic, but also self-similar. Thus, the usual symmetry, translational invariance, has been replaced by invariance with respect to multiplicative changes of scale (scaling invariance). The scaling factor is, of course, equal to 2. Periodicity has always provided a useful tool to understand and simplify the formulation of physical problems (e.g., Bloch's theorem, crystalline momentum conservation). Needless to say, for aperiodic sequences, these tools become powerless. However, the concept of periodicity is still (in a subtle way) lurking behind the Thue-Morse construction because scale invariance is nothing other than periodicity on a logarithmic scale.

The sequence of some TM-chain parameters, such as hopping amplitudes t_s and t_l, is obtained by associating to every 1 and 0 of the above sequence, the values $t_s = 1$ and $t_l = r$, respectively. Therefore, the deviation of r from unity conveniently gauges the lack of translational invariance in the system. In other words, our results will obviously depend on the choice of r. Clearly, the $r \simeq 1$ limit corresponds to the usual periodic regime, while the limits $r \ll 1$ and $r \gg 1$ correspond to the strongly aperiodic regimes. Needless to say, numerical computations cannot handle the infinite aperiodic chain. However, the aperiodic TM structure can be conveniently approximated by a sequence of chains with progressively larger unit cells of sizes 2^n and periodic boundary conditions.

III. ABSENCE OF δ-FUNCTION PEAKS IN THE FOURIER SPECTRUM OF THE THUE-MORSE CHAIN

Let us assume that we have two different types of diffraction centers, with scattering factors f_a and f_b, associated with sites 0 and 1 of the TM chain, respectively. The distance between the neighboring centers is constant, e.g., equal to 1. The scattering properties of such TM chains are described by the function

$$\sum_{n=0}^{2^N-1} f_n \, \delta(x - n) ,$$

where f_n can assume two values, f_a and f_b. The Fourier transform of this function is

$$S_N(\lambda) = \frac{1}{2^N} \sum_{0 \le n \le 2^N - 1} f_n \, e^{2\pi i \lambda n} . \qquad (2)$$

Now the Fourier sum will be split in two groups of terms, and afterwards the relations $f_{2n} = f_n$ and $f_{2n+1} = f_a + f_b - f_n$ directly resulting from the definition (1) of the TM sequence will be used. This results in the relation

$$\begin{aligned} S_N(\lambda) = \ &\tfrac{1}{2}(1 - e^{2\pi i \lambda}) S_{N-1}(2\lambda) \\ &+ (f_a + f_b) \, e^{2\pi i \lambda} \, F(2\lambda, N) , \end{aligned} \qquad (3)$$

where

$$F(\Lambda, N) = \begin{cases} \tfrac{1}{2} & \text{if } \Lambda \text{ is an integer} \\ \dfrac{1}{2^N} \dfrac{1 - e^{i\pi\Lambda 2^N}}{1 - e^{2\pi i \Lambda}} & \text{otherwise.} \end{cases}$$

An alternative way to split the sum of Eq. (2) is to use the relation $f_{2^k+n} = f_a + f_b - f_n$ [corresponding to $\epsilon_{2^k+n} = 1 - \epsilon_n$, which is equivalent to Eq. (1)]. This procedure gives the recursion relation

$$\begin{aligned} S_N(\lambda) = \ &\tfrac{1}{2}(1 - e^{2^N \pi i \lambda}) S_{N-1}(\lambda) \\ &+ (f_a + f_b) e^{2^N \pi i \lambda} F(\lambda, N) . \end{aligned} \qquad (4)$$

The initial condition is

$$S_1(\lambda) = \tfrac{1}{2} e^{\pi i \lambda} \left(f_a e^{-\pi i \lambda} + f_b e^{\pi i \lambda} \right) .$$

Equations (3) and (4) enable us to calculate, for any λ, the scaling of $S_N(\lambda)$ with N as $N \to \infty$. For $f_a + f_b = 0$, it can be easily shown from any of these two equations that for any λ, $S_N(\lambda) \to 0$ as $N \to \infty$. The scaling coefficients of $S_N(\lambda)$ for this case are given in Ref. 9. Thus, the spectrum does *not* have δ-function peaks. For $f_a + f_b \ne 0$, one can obtain immediately from any of the Eqs. (2)–(4) that $S_N(n) = \frac{f_a + f_b}{2}$ for any arbitrary integer n. Thus, there is a periodic array of δ-function peaks situated at integer values of λ. However, such peaks are present in any structure, including a random one, for which $\lim_{L \to \infty} \frac{1}{L} \sum_{k=0}^{L-1} f_k$ is nonzero. Here L is the number of sites in the chain. For all noninteger values of λ, Eqs. (3) and (4) still allow for the solution $\lim_{N \to \infty} S_N(\lambda) = 0$. In this case, Eq. (4) can be cast in the form

$$\begin{aligned} S_N(\lambda) = \ &\tfrac{1}{2}(1 - e^{2^N \pi i \lambda}) \\ &\times \left(S_{N-1}(\lambda) + \frac{f_a + f_b}{2^{N-1}} \frac{e^{2^N \pi i \lambda}}{1 - e^{2\pi i \lambda}} \right) , \end{aligned}$$

which indicates that $S_N(\lambda)^{(f_a + f_b \ne 0)} \propto S_N(\lambda)^{(f_a + f_b = 0)}$ for noninteger λ. Apart from the presence of δ-function peaks at the integer values of λ, the form of $S_N(\lambda)$ seems to be essentially independent of the value of $f_a + f_b$. Our numerical calculations confirm this: for several values of $f_a + f_b$ we have obtained practically the same shape of $S_N(\lambda)$ as depicted in Fig. 1 of Ref. 9 for $f_a = -f_b = 1$.

Therefore, we can conclude that a TM chain with *any* value of $f_a + f_b$ has a spectrum with no δ functions for noninteger values of λ.

In spite of the aperiodicity and the absence of δ-function peaks for noninteger values of λ, the TM Fourier spectrum exhibits very prominent high peaks that would be completely absent in a random sequence. Therefore, the scaling invariance of the system (i.e., periodicity on a logarithmic scale) produces long-range correlations that somewhat mimic, in a very crude way, the behavior of a chain with periodicity.

A few additional remarks might be appropriate. Equation (2) is not the only way to define the structure factor corresponding to a substitutional sequence. Another possibility is to arrange identical scatterers (e.g., with $f_n = 1$) in such a way that the distances between the neighboring scatterers can assume only two values that are alternated according to a certain sequence (e.g., Thue-Morse or Fibonacci). The structure factor is then given by the Fourier transform of the density

$$\rho(x) = \sum_k \delta(x - x_k) \, ,$$

where x_k are the positions of the scatterers and the differences $x_k - x_{k-1}$ can assume two values; e.g., for Thue-Morse sequence one could put

$$x_k - x_{k-1} = l_0 + \epsilon_k \, \Delta l \, ,$$

where l_0 and Δl are some suitable constants. Structure factors of this type were investigated for various sequences in Refs. 25–28. For instance, Ref. 29 contains a proof that the Thue-Morse lattice defined in this way is not quasiperiodic. A general case would then be represented by varying simultaneously both the distance of neighboring scatterers and their scattering factors. Moreover, the scattering power of the same scatterers can be different for different types of scattered particles or waves.

IV. WHERE THE SPECTRAL GAPS ARE AND WHAT THEIR RELATIVE SIZES ARE: ANALYTICAL APPROACH BASED ON DEGENERATE PERTURBATION THEORY

An extremely simple argument based on perturbation theory is sufficient to predict the location and relative magnitude of the spectral gaps in the Thue-Morse, or any other aperiodic, chain. Let us first consider the problem of solving for the excitation spectrum of a Thue-Morse nearest-neighbor hopping Hamiltonian on N sites in the perturbative regime, where the small parameter is the difference in the transition energies between the short and long segments, i.e., $| t_s - t_l |$. The locations and sizes of the gaps do not depend on boundary conditions.[15] Therefore, for convenience, we choose here periodic boundary conditions as for the moment we are only interested in the locations and sizes of gaps, not in the nature of the eigenstates in the gaps. We first write our Hamiltonian as $H = H^0 + H'$, where

$$H^0_{ij} = t_0(\delta_{i,j+1} + \delta_{i+1,j}) \quad (i,j = 1,2,\ldots,N) \tag{5}$$

and

$$H'_{ij} = t_i \, \delta_{i+1,j} + t_j \, \delta_{i,j+1}. \tag{6}$$

Note that the i,j indices identify $N+1$ with 1. The entries in H', t_i, are chosen in a Thue-Morse sequence and are considered to be small compared to t_0. For reasons that will become clear later we will also require that the entries of H' satisfy

$$\sum_{n=1}^{N} t_n = 0. \tag{7}$$

For a given H it is always possible to find a t_0 such that Eq. (7) is satisfied. Now, the states that diagonalize H^0 are, of course, given by

$$| n \rangle = \frac{1}{\sqrt{N}}(e^{ik_n}, e^{i2k_n}, \ldots, e^{iNk_n})$$

for n satisfying $-N/2 < n \le N/2$, where $k_n = 2\pi n/N$, and their eigenvalues are given by

$$\epsilon^0(k_n) = 2t_0 \cos(k_n). \tag{8}$$

Note the degeneracy in Eq. (8) between time-reversed states $| n \rangle$ and $| -n \rangle$. The matrix elements of H' in this basis are given by

$$\langle n \mid H' \mid m \rangle = 2\, t(k_m - k_n)$$
$$\times \cos\left(\frac{k_n + k_m}{2}\right) \, e^{\frac{i}{2}(k_m - k_n)},$$

where

$$t(k_m - k_n) = N^{-1} \sum_{p=1}^{N} t_p \, e^{ip(k_m - k_n)} \, . \tag{9}$$

Note that from Eq. (7), $\langle n \mid H' \mid n \rangle = 0$. If we now perform first-order degenerate perturbation theory with the states $| n \rangle$ and $| -n \rangle$, we find that the eigenenergies of H are given to this order by

$$\epsilon^{\pm}(k_n) = 2\left[t_0 \cos(k_n) \pm |t(2k_n)|\right] \, . \tag{10}$$

Comparison of this result with the numerical calculation of the location and magnitude of the gaps in the phonon spectrum show an excellent agreement among them. This has been originally pointed out, for aperiodic sequences, in the first paper of Ref. 15. Note that Fig. 4 in that paper is similar, but obviously not equal, to a structure factor. The only extra feature present there, for the phonon case, and absent here is the presence of Goldstone modes, which suppress the gap size for long-wavelength excitations. Also, in the quantum Ising model to be studied below, there is a suppression of gap sizes for long-wavelength excitations.

V. GENERALIZED THUE-MORSE CHAINS

One can generalize the Thue-Morse sequence in a way similar to the generalization of the Fibonacci sequence.[17] We will define two sequences of strings by the following inflation scheme

$$A_{l+1} = A_l^m B_l^n \, , \quad B_{l+1} = B_l^n A_l^m \, , \tag{11}$$

where $A_0 \equiv 0$, $B_0 \equiv 1$, m and n are integers, and A_l^m represents m adjacent repetitions of the string A_l, etc. Then the infinite string of 0's and 1's defined by $\lim_{l \to \infty} A_l$ is called a generalized Thue-Morse (GTM) sequence. In analogy with the Fibonacci case, A_l will be called the lth GTM generation. Let us note that our generalization differs from that of Keane[20] based on more than two symbols. The inflation scheme of Eq. (11) is equivalent to the substitution rule $0 \to 0^m 1^n$, $1 \to 1^n 0^m$, where 0^m represents a string of m 0's, etc. Both strings A_l and B_l have the same length equal to $(m+n)^l$. Let us denote by $N_l(0)$ and $N_l(1)$ the numbers of 0's and 1's contained in A_l. For $l > 0$, the same numbers pertain also to B_l and we have $N_l(0) = m(m+n)^{l-1}$ and $N_l(1) = n(m+n)^{l-1}$. Thus for all GTM sequences,

$$\frac{N_l(0)}{N_l(1)} = \frac{m}{n} \, ,$$

which is independent of l. This implies that, unlike cases such as the golden-mean Fibonacci sequence in the limit $l \to \infty$, an irrational ratio can never be obtained for the GTM sequences. In this aspect, as well as in the fact that the dimensionality of their trace maps is two, as will be shown in the next section, all GTM sequences resemble the $n = m+1$ subset of the generalized Fibonacci sequences.[11]

VI. TRACE MAPS OF THE GENERALIZED THUE-MORSE SEQUENCES

Let us assume that the 0's and 1's that constitute the GTM sequence represent two different building blocks, such as atoms or two-dimensional layers. We will limit ourselves to the class of physical properties that can be studied in terms of 2×2 transfer matrices of unit determinant. Denoting the whole transfer matrix of the chain (superlattice) A_l as $\mathcal{M}_l$ and that of B_l as $\mathcal{N}_l$, the matrix equivalent of Eq. (11) is

$$\mathcal{M}_{l+1} = \mathcal{N}_l^n \mathcal{M}_l^m, \quad \mathcal{N}_{l+1} = \mathcal{M}_l^m \mathcal{N}_l^n \, , \tag{12}$$

where $\mathcal{M}_0$ and $\mathcal{N}_0$ are the transfer matrices of the two basic building blocks 0 and 1, respectively. In the periodic approximation in which A_l serves as a unit cell of a periodic chain, which is called the lth periodic approximant of the infinite TM chain, the allowed energies or frequencies are given by the condition

$$-1 \leq x_l \leq 1 \, , \tag{13}$$

where $x_L = \frac{1}{2} \mathrm{Tr}(\mathcal{M}_l)$. For $l > 0$, $\mathrm{Tr}(\mathcal{M}_l) = \mathrm{Tr}(\mathcal{N}_l)$.

Our aim is to express x_l in terms of the previous traces x_k, $k < l$. We will proceed along the same lines as in our recent work[11] in which we derived the trace maps for the generalized Fibonacci sequences. (The proof that trace maps exist for arbitrary two-letter substitutional sequences was for the first time presented by Allouche and Peyrière.[30]) We will need the following formula:[11]

$$\mathrm{Tr}(\underline{a}^k \underline{b}) = \mathrm{Tr}(\underline{b}\, \underline{a}^k) = d_k(\xi) \, \mathrm{Tr}(\underline{a}\, \underline{b}) - d_{k-1}(\xi) \, \mathrm{Tr}\, \underline{b} \, , \tag{14}$$

where $\underline{a}$ and $\underline{b}$ are 2×2 matrices such that $\det \underline{a} = 1$, $\xi = \mathrm{Tr}\, \underline{a}$, k is an arbitrary integer (positive or negative), and $d_k(\xi)$ is a polynomial in ξ such that

$$d_{k+1}(\xi) = \xi \, d_k(\xi) - d_{k-1}(\xi) \, , \quad d_0(\xi) \equiv 0 \, , \quad d_1(\xi) \equiv 1 \, .$$

Thus, $d_2(\xi) = \xi$, $d_3(\xi) = \xi^2 - 1$, $d_4(\xi) = \xi^3 - 2\xi$, etc. For positive k, we have $d_k(\xi) = S_{k-1}(\xi) = U_{k-1}(\xi/2)$, where $S_j(\xi)$ and $U_j(\xi)$ are Chebyshev polynomials of the first and second kind. Among others, the d polynomials have the following properties:

$$d_k(2) = k \, , \quad d_k(-2) = (-1)^{k+1} \, ,$$

$$d_{2k}(0) = 0 \, , \quad d_{2k+1}(0) = (-1)^k \, ,$$

and

$$d_{-k} = -d_k \, ,$$

$$d_k d_{l+1} - d_{k-1} d_l = d_{l+k} \, ,$$

$$d_{l+k} - d_{l-k} = d_k (d_{l+1} - d_{l-1}) \, ,$$

$$d_{k+l} d_{k-l} = d_k^2 - d_l^2 \, ,$$

$$\frac{d}{d\xi}(d_{k+1} - d_{k-1}) = k \, d_k \, ,$$

where the argument of all the d polynomials is the same.[11]

Using Eq. (12), one can write

$$x_{l+1} = \frac{1}{2} \mathrm{Tr}(\mathcal{M}_{l+1}) = \frac{1}{2} \mathrm{Tr}(\mathcal{N}_l^n \mathcal{M}_l^m) \, . \tag{15}$$

Applying Eq. (14) twice, we get [cf. Eqs. (9) and (10) of Ref. 11]

$$x_{l+1} = d_m(2x_l)[d_n(2x_l) \tfrac{1}{2} \mathrm{Tr}(\mathcal{M}_l \mathcal{N}_l) - d_{n-1}(2x_l) \, x_l]$$

$$- \tfrac{1}{2} d_{m-1}(2x_l)[d_{n+1}(2x_l) - d_{n-1}(2x_l)],$$

which can be further simplified to

$$x_{l+1} = d_m(2x_l) \, d_n(2x_l) \, [\tfrac{1}{2} \mathrm{Tr}(\mathcal{M}_l \mathcal{N}_l) - 1]$$

$$+ \tfrac{1}{2} [d_{n-m+1}(2x_l) + d_{m-n+1}(2x_l)] \, . \tag{16}$$

The form of Eq. (16) suggests that a suitable choice for the second "trace coordinate" is $y_l = \frac{1}{2}\mathrm{Tr}(\mathcal{M}_l\mathcal{N}_l)$. Using Eq. (12), one can write

$$y_{l+1} = \frac{1}{2}\mathrm{Tr}(\mathcal{M}_{l+1}\mathcal{N}_{l+1}) = \frac{1}{2}\mathrm{Tr}(\mathcal{N}_l^{2n}\mathcal{M}_l^{2m}) .$$

Comparing this with Eq. (15), one can see immediately that the recursion formula for y_{l+1} can be obtained from Eq. (16) by substituting $2m$ for m and $2n$ for n. Thus, the trace maps of the GTM sequences are *two dimensional* and have the form

$$x_{l+1} = d_m(2x_l)\,d_n(2x_l)\,(y_l - 1)$$
$$+ \tfrac{1}{2}\,[d_{n-m+1}(2x_l) + d_{m-n+1}(2x_l)] ,$$

$$y_{l+1} = d_{2m}(2x_l)\,d_{2n}(2x_l)\,(y_l - 1)$$
$$+ \tfrac{1}{2}\,[d_{2n-2m+1}(2x_l) + d_{2m-2n+1}(2x_l)] , \qquad (17)$$

where $l > 0$. Initial conditions are

$$x_0 = \tfrac{1}{2}\mathrm{Tr}(\mathcal{M}_0) ,\ \bar{x}_0 = \tfrac{1}{2}\mathrm{Tr}(\mathcal{N}_0) ,\ y_0 = \tfrac{1}{2}\mathrm{Tr}(\mathcal{M}_0\mathcal{N}_0) ,$$

$$x_1 = d_m(2x_0)\,d_n(2\bar{x}_0)\,y_0 - \tfrac{1}{2}\,[\ d_{m-1}(2x_0)\,d_{n+1}(2\bar{x}_0)$$
$$+ d_{m+1}(2x_0)\,d_{n-1}(2\bar{x}_0)] ,$$

$$y_1 = d_{2m}(2x_0)\,d_{2n}(2\bar{x}_0)\,y_0 \qquad\qquad (18)$$
$$- \tfrac{1}{2}\,[d_{2m-1}(2x_0)\,d_{2n+1}(2\bar{x}_0)$$
$$+ d_{2m+1}(2x_0)\,d_{2n-1}(2\bar{x}_0)] .$$

For $m = n$, Eqs. (17) reduce to a very simple form,

$$x_{l+1} = [d_n(2x_l)]^2\,(y_l - 1) + 1 ,$$

$$y_{l+1} = [d_{2n}(2x_l)]^2\,(y_l - 1) + 1 , \qquad (19)$$

which for the original TM chain, $m = n = 1$, further reduces to

$$x_{l+1} = y_l ,\quad y_{l+1} = 4x_l^2\,(y_l - 1) + 1 , \qquad (20)$$

which is identical with the map obtained by Axel *et al.*[5]

Note that for arbitrary m and n, Eqs. (17) maps a straight line $x_l = \xi$ =const onto an inclined straight line with the slope

$$\frac{d_{2m}(2\xi)\,d_{2n}(2\xi)}{d_m(2\xi)\,d_n(2\xi)} = [d_{m+1}(2\xi) - d_{m-1}(2\xi)]\,[d_{n+1}(2\xi) - d_{n-1}(2\xi)]$$

that goes through the point

$$P = \left(\tfrac{1}{2}\,[d_{n-m+1}(2\xi) + d_{m-n+1}(2\xi)],\ \tfrac{1}{2}\,[d_{2n-2m+1}(2\xi) + d_{2m-2n+1}(2\xi)]\right) .$$

If $d_n(2\xi) = 0$ or $d_m(2\xi) = 0$, the whole image of the $x_l = \xi$ line shrinks just to the point P. For arbitrary ξ, point P lies on the parabola $y = 2x^2 - 1$ as can be verified by direct calculation.

The Jacobian of the map (17) is

$$J = (n - m)\,(d_{2n}\,d_{2m}\,d_{n-m} - 2\,d_n\,d_m\,d_{2n-2m}) - 2(y_l - 1)\,d_n\,d_m\,(n\,d_n^2\,d_{2m} + m\,d_m^2\,d_{2n}) ,$$

where the argument of all d polynomials equals $2x_l$. Apparently, for all m and n, $|J| \not\equiv 1$. Thus, this map is *area nonpreserving*.

It is also evident from Eq. (17) that it is noninvertible. Let us assume that x_{l+1} and y_{l+1} in Eq. (17) are given, and x_l and y_l are unknown. After eliminating y_l one gets an equation of the $[2\max(m,n)]$th order for x_l. Thus, a general point can have between zero and $2\max(m,n)$ predecessors depending on the number of real roots of this equation. Moreover, for each m and n, there is at least one point that has infinitely many predecessors. (i) For $m = n$, it is the point $(1,1)$. Among its predecessors are all points on the line $y = 1$. (ii) For $m+n$ =odd, it is the point $(0,-1)$. Among its predecessors are all points on the line $x = 0$. (iii) When both m and n are even, it is the point $((-1)^{\frac{m-n}{2}}, 1)$. Among its predecessors is again the whole line $x = 0$. In all these three cases the respective points listed above are fixed points. (iv) In the remaining case, when both m and n are odd and $m \neq n$ (i.e., at least one of them is different from one), we will use the fact that for $k > 1$ there are always real solutions

of the equation $d_k(2\xi) = 0$. Thus all the points P mentioned above corresponding to $d_m(2\xi) = 0$ or $d_n(2\xi) = 0$ will have infinitely many predecessors. These predecessors are all the points on the $x = \xi$ line. Several such points may, of course, exist also in the previous three cases. However, they will generally not be fixed points. Actually, the points given above in (ii) and (iii) are special cases of the P points corresponding to the root $\xi = 0$.

VII. ATTRACTOR OF THE GENERALIZED THUE-MORSE MAPS

The TM map of Eq. (20) has some similarity with the copper-mean map for $\gamma = -1$ whose invariant curve in certain trace coordinates is a parabola.[12] This led us to investigate the following quantity:

$$U_l = y_l - 2\,x_l^2 + 1 . \qquad (21)$$

Using Eq. (17), one can find that U_l transforms as

$$U_{l+1} = 2\,[d_m(2x_l)]^2\,[d_n(2x_l)]^2\,(1 - y_l)\,U_l . \qquad (22)$$

It is obvious that U_l is not exactly a pseudoinvariant as defined in Refs. 31 and 12 because its sign can change. However, we will see that it is equally important. First of all, the set of points satisfying $U_l = 0$ is clearly an invariant set. During iterations of the GTM maps, points cannot escape from this set, but new points can end up in it via the $y = 1$ line or the zeros of the d_m and d_n polynomials. This invariant set is the parabola $y = 2x^2 - 1$. It contains all the fixed points mentioned in the preceding section. This parabola also contains all the P points introduced above as can be seen directly from Eq. (22) because these points are the images of the points with $y_l = 1$. Thus it contains all the points with an infinite number of predecessors. All these predecessors are attracted to the $U_l = 0$ set from "afar." We will show that the $y < 1$ part of the $U_l = 0$ parabola, i.e., the set $\mathcal{A} \equiv \{|x| \leq 1, y = 2x^2 - 1\}$, is an attractor of the same type as those investigated in Ref. 12 for the generalized Fibonacci maps. It is interesting that the attractor is the same for all GTM maps. The same situation was obtained in the case of generalized Fibonacci maps when suitable coordinates were introduced.[11]

The expression for y_{l+1} of Eq. (17) can be cast in the form

$$y_{l+1} - 1 = [d_{m+n}(2x_l)]^2 (y_l - 1) - [d_{n-m}(2x_l)]^2 U_l .$$
(23)

Equations (22) and (23) divide the whole trace space into four different regions:

I : $y \leq 1$ and $y \geq 2x^2 - 1$ $(U_l \geq 0)$,

II : $y > 1$ and $y > 2x^2 - 1$ $(U_l > 0)$,

III : $y < 1$ and $y < 2x^2 - 1$ $(U_l < 0)$,

IV : $y > 1$ and $y < 2x^2 - 1$ $(U_l < 0)$.

Region I is an invariant bounded region that is fully contained within the $\{|x| \leq 1, |y| \leq 1\}$ square. This square corresponds according to Eq. (13) to the allowed energies (frequencies). Region I is thus an equivalent of the Lissajous curve and its interior of the Fibonacci copper-mean map.[12] According to Eqs. (22) and (23), points cannot escape from region I. However, points from its interior can end up on $\mathcal{A}$ (parabolic part of the boundary of region I) where they will stay forever. Thus, if in a whole interval of energies (frequencies) the initial values (x_1, y_1) of the GTM traces were situated in region I, one would obtain a continuous allowed band similar to those of periodic crystals. However, it seems that for a truly nonperiodic crystal, an initial point can never lie in the interior of region I. Substituting into Eq. (21) for (x_1, y_1) from Eq. (18), one can easily calculate U_1. After some manipulation, one gets

$$U_1 = -2 [d_m(2x_0)]^2 [d_n(2\bar{x}_0)]^2 I ,$$
(24)

where $I = \bar{x}_0^2 + x_0^2 + y_0^2 - 2\bar{x}_0 x_0 y_0 - 1$ is the value of

the Fibonacci golden-mean map invariant [and the (initial) value of the (pseudo)invariants of all generalized Fibonacci maps in the second (with tilde) set of coordinates of Ref. 11] that corresponds to a Fibonacci system constructed with the same building blocks as our GTM system [cf. Eq. (18)]. In all previous studies of the Fibonacci quasiperiodic *crystals*, it never happened that I was negative and the initial point was at the same time inside the central bounded spherelike portion of the $I = 0$ surface (i.e., in the notation of this section, the conditions $I < 0$ and $|x_0| < 1$, $|\bar{x}_0| < 1$, and $|y_0| < 1$ were never satisfied simultaneously—see the discussion on this matter in Refs. 12 and 31). A case of negative I was reported earlier by Sutherland[32] who investigated the dynamics of a *spin* placed in quasiperiodically pulsed magnetic field. However, in this dynamics of a spin, the "transfer" matrices are such that their traces are always less than 2, and hence the corresponding points in the trace space must always be inside the central bounded portion of the $I = 0$ surface. In crystals of arbitrary structure (periodic, QP, or random), a similar situation would correspond to all energies (frequencies) being allowed. Thus such a dynamical system has little in common with crystals and cannot be used to model them. Using Eqs. (18) and (24) one can find that for arbitrary m and n there is a one-to-one correspondence between the interior of the central bounded portion of the $I = 0$ surface and the interior of region I. Thus we can expect that the initial points will never lie in the interior of region I. This will be demonstrated by a few examples in the following sections. However, Eq. (24) suggests that the initial point can lie in the $\mathcal{A}$ set if $2x_0$ or $2\bar{x}_0$ happens to be a root of polynomial d_m or d_n, respectively. Around the energies (frequencies) corresponding to such values of $2x_0$ or $2\bar{x}_0$ we expect "Bloch-like" bands as observed in Refs. 31 and 12.

According to Eqs. (22) and (23), points from region II will in the next iteration appear in region III or IV, points from region III will jump into region II, and points from region IV will stay there or jump into region III. For $m = n$ the motion of points is restricted even more: no points can cross the $y = 1$ line as the second term of Eq. (23) is identically zero in this case. This can also be seen directly from Eq. (19). Regions II, III, and IV will contain mostly escaping points, some periodic orbits (although most of the periodic orbits can be expected in region I) and an infinite (though probably of zero measure) set of points whose descendents will eventually end up in the $\mathcal{A}$ set. According to Eq. (22) such a set can be constructed by looking successively for all predecessors of the $y = 1$ line and those lines $x = \xi$ where ξ is a root of the d_m or d_n polynomial. The simplest situation occurs for $m = n = 1$ when d_1 has no roots, and it is sufficient to investigate the predecessors of the $y = 1$ line only. The 11 generations of predecessors of this line are shown in Fig. 1. In the case of the original TM sequence all those points that are ending up in the $\mathcal{A}$ set come through the $(1, 1)$ point where they remain, as it is a fixed point. Thus only this point actually plays the role of the attrac-

tor for $m = n = 1$. For the general case the situation will be more complex as there may be more entry points into the $\mathcal{A}$ set and the attracted points can diffuse along the whole $\mathcal{A}$ set. The basin of attraction of Fig. 1 has similar fractal character as that of the copper-mean map attractor.[12] Some details of this structure are revealed in Fig. 6(b). Also, in the $m = n = 1$ case, one can prove that all points $y > 1$, $x \neq 0$ do escape to infinity. That is why there are no lines of predecessors of the $(1,1)$ point in this region. Thus any initial point of the trace map lying in this region must correspond to a gap.

In the end let us note that if we introduce another quantity $T_l = 1 - y_l$, the pair T_l and U_l can play the role of new trace coordinates. We can rewrite Eqs. (22) and (23) as

$$T_{l+1} = [d_{m+n}(2x_l)]^2 \, T_l + [d_{n-m}(2x_l)]^2 \, U_l \ ,$$

$$U_{l+1} = 2 \, [d_m(2x_l)]^2 \, [d_n(2x_l)]^2 \, T_l \, U_l \ .$$

For any k, $[d_k(\xi)]^2$ is a polynomial in ξ^2 only. Thus we can substitute without any problems into the above

equations $4x_l^2 = 2\,(2 - T_l - U_l)$ and then we really obtain a map in T_l, U_l coordinates only. In this coordinate system, the four regions defined above are simply intersections of the four quadrants with the $T_l + U_l \leq 2$ half plane. For example, region I becomes the triangle with vertices $(0,0)$, $(0,2)$, and $(2,0)$. The $T_l + U_l > 2$ half plane does not correspond to any point in the old x_l, y_l coordinates.

VIII. ELECTRONIC AND SPIN EXCITATIONS IN THE THUE-MORSE SEQUENCE

Figure 1 represents the properties of the TM map as given by Eq. (20). It is completely independent of the nature and the properties (parameters) of the building blocks 0 and 1. To estimate quite accurately the energy spectrum for a particular model with the TM lattice such that its building blocks can be associated with certain 2×2 unimodular transfer matrices, it is sufficient to plot into Fig. 1 the initial values (x_1, y_1) of traces as the function of energy and find the energies corresponding to the intersections of the locus of initial points (x_1, y_1)
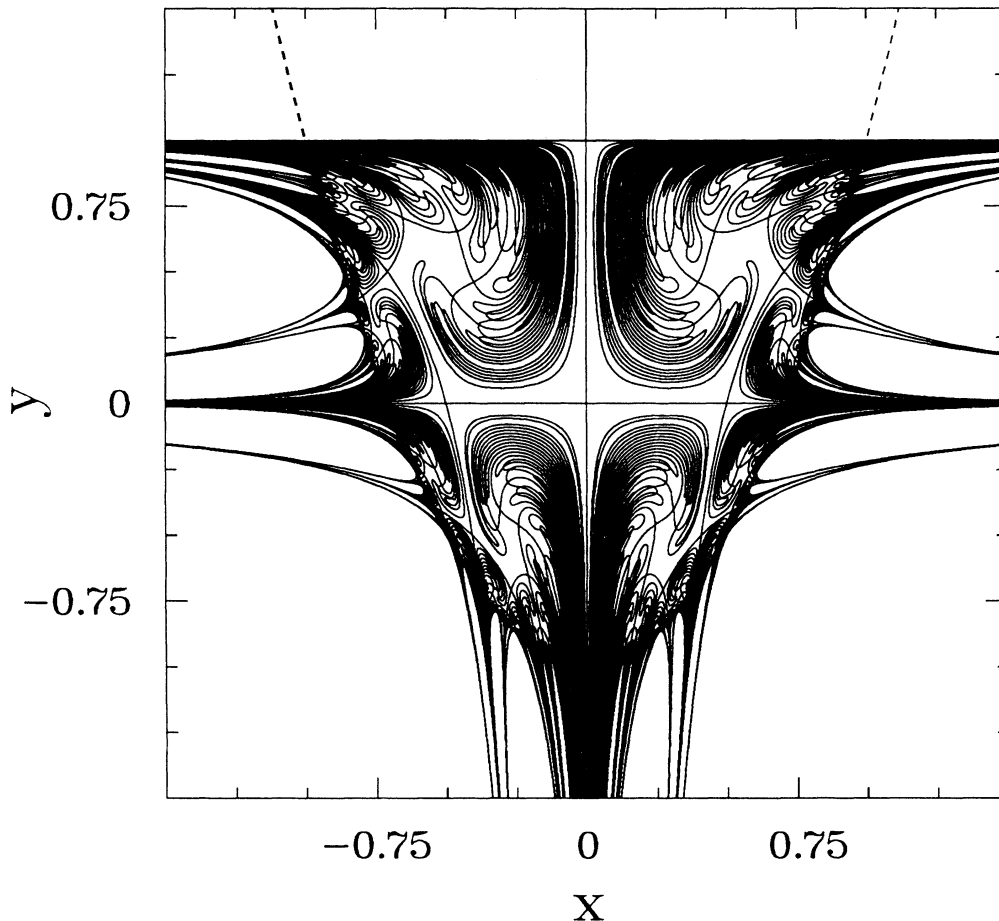

FIG. 1.   Thue-Morse map $(m = n = 1)$. The first 12 generations of the predecessors of the $(1,1)$ point (solid lines) are shown. The invariant parabola $(y = 2x^2 - 1)$ is plotted by the dashed line.

with various parts (beams of lines) of the fractal basin of attraction of Fig. 1. In this section we will do that for two cases: (i) the electronic spectra of the "diagonal" tight-binding model[8] and (ii) the quantum Ising model.[7] We will show that in this way one can predict the structure of spectra as obtained in Refs. 8 and 7 *without* going through the iterations of the TM trace map.

A. The diagonal model

Let us consider a TM chain of atoms characterized by two different values of the diagonal matrix elements of the potential, V and $-V$, associated with sites of type 0 and 1, respectively, and by the same hopping matrix element equal to -1 for all nearest neighbors. For this choice,[8] the two initial matrices of Eqs. (12) and (18) are (cf. Refs. 16 and 12)

$$\mathcal{M}_0 = \begin{pmatrix} V-E & -1 \\ 1 & 0 \end{pmatrix} \ , \quad \mathcal{N}_0 = \begin{pmatrix} -V-E & -1 \\ 1 & 0 \end{pmatrix} \ ,$$

where E is the energy. Thus $\bar{x}_0 = -(V+E)/2$, $x_0 = (V-E)/2$; $y_0 = (E^2-V^2-2)/2$, and the Fibonacci invariant occurring in Eq. (24) is $I = V^2$. Because I is not dependent on energy in the diagonal model, we find from Eq. (24) that $U_1 = -2V^2$ is also energy independent. Thus the locus of initial points lies on a parabola that can be obtained by shifting the invariant parabola $y = 2x^2 - 1$ downward by $-U_1 = 2V^2$. It is the set

$$y_1 = 2x_1^2 - 1 - 2V^2 \ , \quad x_1 > -\frac{V^2+2}{2} \ . \tag{25}$$

From Eq. (18), the dependence of x_1 on energy is $x_1 = y_0 = (E^2 - V^2 - 2)/2$.

For large negative energies E, $x_1 \gg 0$ and $y_1 \gg 0$. As the energy increases, the initial point of the trace map moves down along the parabolic segment of Eq. (25) and intersects successively all the beams of lines of the predecessors of the $(1,1)$ point. For $E = -\sqrt{V^2+2}$, the initial point reaches the bottom of the parabolic segment, and for $E = 0$, it is in the highest point, $(-1-\frac{1}{2}V^2, 1+\frac{1}{4}V^4)$, of the left branch of the segment of Eq. (25). The increase of the height of the $E = 0$ initial point above the $y = 1$ line with increasing V corresponds in Fig. 1 of Ref. 8 to the widening of the central gap (remember that all points $y > 1$, $x \neq 0$ are escaping). As the energy increases further into the range of positive values, the initial point travels along the same parabola in the opposite direction thus giving rise to the mirror symmetry of the energy spectra in Figs. 1 and 2 of Ref. 8 with respect to the $E = 0$ point.

The bottom of the lowermost energy band and the top edge of the uppermost one obviously correspond to $y_1 = 1$ and positive x_1, which according to Eq. (25) must be $x_1 = \sqrt{V^2+1}$. This gives immediately their dependence on V in the form

$$E = \pm \left[2\left(1 + \sqrt{1+V^2}\right) + V^2 \right]^{\frac{1}{2}} \ .$$

Similarly, the edges of the central gap correspond to $y_1 = 1$ and $x_1 = -\sqrt{V^2+1}$, giving

$$E = \pm \left[2\left(1 - \sqrt{1+V^2}\right) + V^2 \right]^{\frac{1}{2}} \ .$$

The centers of the other gaps correspond roughly to the intersections of the initial-point parabolic segment of Eq. (25) with the $y = 0$ and $x = 0$ lines. These intersections correspond to

$$E = \pm \left[2\left(1 + \sqrt{\tfrac{1}{2}+V^2}\right) + V^2 \right]^{\frac{1}{2}} \ ,$$

$$E = \pm \left[2\left(1 - \sqrt{\tfrac{1}{2}+V^2}\right) + V^2 \right]^{\frac{1}{2}} \ ,$$

and

$$E = \pm\sqrt{2+V^2} \ .$$

All these formulas are in perfect agreement with Figs. 1 and 2 of Ref. 8.

B. The quantum Ising model

Let us now try to explain in the same way the spectrum of the TM quantum Ising chain in the transverse field.[7] The transverse magnetic field is assumed equal to unity. The nearest-neighbor exchange interaction can assume two values, λ associated with 0's in the TM string and $r\lambda$ associated with 1's. Then the initial conditions from Eqs. (18) can be shown to be

$$\bar{x}_0 = \frac{E^2/4 - (1 + r^2\lambda^2)}{2r\lambda} \ , \quad x_0 = \frac{E^2/4 - (1+\lambda^2)}{2\lambda} \ ,$$

$$y_0 = 2\bar{x}_0 x_0 - \frac{1}{2}\left(r + \frac{1}{r}\right) \ ,$$

$$x_1 = y_0 \ , y_1 = 1 - 2\bar{x}_0^2 - 2x_0^2 + 4\bar{x}_0 x_0 y_0$$

(cf., e.g., Ref. 33). In this case the dependence of y_1 on x_1 cannot be written in a simple explicit form. However, we can easily calculate the Fibonacci invariant for the same building blocks, which gives

$$I = \frac{1}{16}\left(r - \frac{1}{r}\right)^2 E^2 \ .$$

From Eq. (24) we have that the set of initial points of the TM map must in this case again have an empty intersection with the interior of region I. The invariant I, and thus also U_1, depends on energy; hence the set of initial points is a complicated curve as depicted in Fig. 2. This figure corresponds to $\lambda = 8/5$ and $r = 1/2$. For several points along the curve of initial values (x_1, y_1), mostly the intersections with various groups of lines of predecessors of the $(1, 1)$ point, the corresponding energy values are indicated. They are fully in agreement with Fig. 3(a) and Table I of Ref. 7. One can show that for arbitrary

λ and r the initial point corresponding to $E=0$ always lies on the invariant parabola $y=2x^2-1$. It always lies *above* the $y=1$ line (i.e., in a purely escaping region) except for the critical value $\lambda=\lambda_c=\sqrt{2}$ for which it falls onto the $(1,1)$ fixed point. Thus only at criticality does the zero-energy gap disappear, as it should.

IX. LIGHT TRANSMISSION THROUGH A THUE-MORSE MULTILAYER

Considering practical applications of one-dimensional models, studies of transmission of light through multilayer media are quite appealing.[34] In this section we
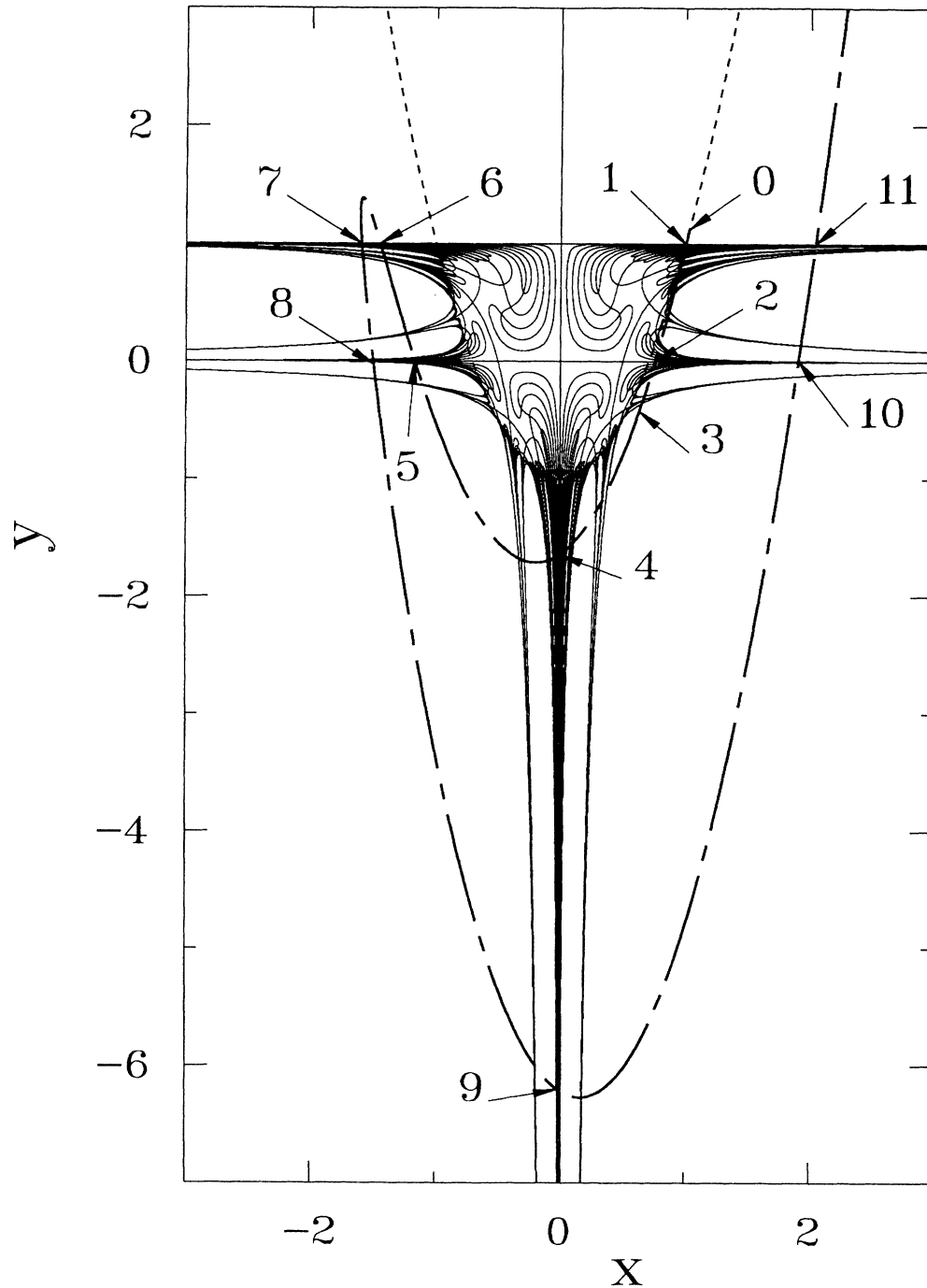
FIG. 2. Same as Fig. 1 except that only nine generations of predecessors of the $(1,1)$ point are plotted. The long and short dashed line represents the set of initial points (x_1, y_1) for the TM map corresponding to the quantum Ising model in the transverse field with $\lambda = 1.6$, $r = 0.5$. The arrows point to the initial points (x_1, y_1) corresponding to the following energies: 0 — 0, 1 — 0.230 44, 2 — 0.74, 3 — 0.9, 4 — 1.51, 5 — 2.48, 6 — 2.8, 7 — 3.3273, 8 — 3.54, 9 — 4.3, 10 — 4.734, 11 — 4.757 73.

present results for the transmission of a transverse electric wave through a multilayer medium, which is constructed by arranging two types of layers according to the Thue-Morse sequence. Unlike the previous studies[34] of light transmission through multilayer media with volume preserving trace maps, the transmissivity of light in the present case can be understood, as shown below, with the help of the associated basin of attractor. We assume that the incident wave travels through a homogeneous medium of refractive index n_0, and after transmission through the multilayer construct, light is measured in a homogeneous medium of refractive index n_l.

Let the refractive index and the thickness of the jth layer be n_j and h_j, respectively. If θ_j is the angle that the light makes with the normal when traveling through the jth layer, the amplitudes of the field vectors on the two sides of the layer can be related by using the transfer matrix[35]

$$\mathbf{M}(h_j) = \begin{pmatrix} \cos\beta_j & -i\,p_j^{-1}\sin\beta_j \\ -i\,p_j\sin\beta_j & \cos\beta_j \end{pmatrix},$$

where $\beta_j = k\,n_j\,h_j\cos\theta_j$, $p_j = n_j\cos\theta_j$, and k is the wave number in vacuum. The transfer matrix corresponding to N layers is

$$\mathbf{M}_N = \prod_j^N \mathbf{M}(h_j) = \begin{pmatrix} M_{11} & M_{12} \\ M_{21} & M_{22} \end{pmatrix}.$$

If p_0 and p_l are the values of p_j corresponding to the incident and transmitted waves, respectively, then the transmissivity T is given by[35]

$$T = 4\,p_0\,p_l\,[\,p_0^2\,M_{11}^2 + p_l^2\,M_{22}^2 + (p_0\,p_l)^2\,|M_{12}|^2$$
$$+ |M_{21}|^2 + 2\,p_0\,p_l\,]^{-1}. \qquad (26)$$

Let the refractive indices of the two basic layers of a TM multilayer be n_A and n_B ($A \equiv 0$, $B \equiv 1$ in the language of Sec. II). For simplicity we consider only normal incidence ($\theta_j = 0$, $p_j = n_j$ for all j), and it is also assumed that the refractive indices and thicknesses are such that $\beta_j = \beta$ for all j. The transfer matrix $\underline{M}_A$ for the layer A is

$$\underline{M}_A = \begin{pmatrix} \cos\beta & -i\,n_A^{-1}\sin\beta \\ -i\,n_A\sin\beta & \cos\beta \end{pmatrix}. \qquad (27)$$

The corresponding matrix $\underline{M}_B$ for the B layer is obtained by replacing the symbol A by B. Thus the transfer matrices for the first two generations of the TM lattice are $\mathcal{M}_1 = \underline{M}_B\underline{M}_A$ and $\mathcal{M}_2 = \underline{M}_B\underline{M}_A\underline{M}_A\underline{M}_B$. The transfer matrices of the higher generations are obtained from the scheme given in Eq. (12) for $m = n = 1$. For sample A and B layers, the transmissivity for six and seven generations are given in Figs. 3 and 4, respectively. These figures show that the transmissivity as a function of β has peaks and the number of these peaks increases with the increase of the generation number. It is not hard to understand this feature of T. The trace map of Eq. (20) shows that $x_{l+2+k} = 1$ for all positive k if $x_l = 0$ and/or $x_{l+1} = 1$. For the TM multilayer medium with the transfer matrices of the two basic layers given by Eq. (27), it can be shown that the transfer matrix for all $l+2+k$ gener-
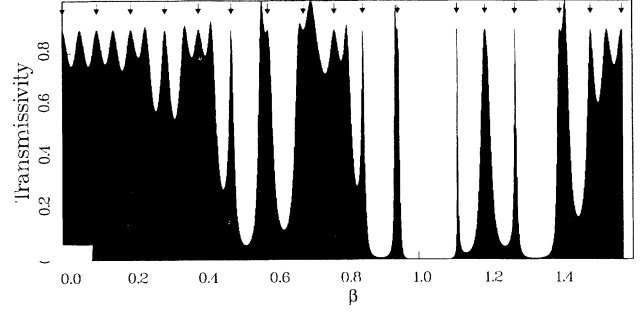

FIG. 3. Plot of the transmissivity T as a function of β for normal incidence. The Thue-Morse multilayer medium has six generations and the parameters are chosen as $n_0 = 1$, $n_A = 2$, $n_B = 3$, and $n_l = 3$. The small arrows pointing downward from the top of the figure indicate the location of β values which give rise to an identity transfer matrix for the multilayer of six generations.

ations becomes an identity matrix if the trace becomes 1 as described above. Thus the transmissivity of Eq. (26), for those values of β that give rise to an identity transfer matrix, is a constant given by $T_c = 4\,p_0\,p_l\,(p_0 + p_l)^{-2}$. This means that for every generation there is a definite number of peaks of height T_c. For six and seven generations, there are 17 and 33 such values of β as shown in Figs. 3 and 4 by small arrows pointing downward from the top of these figures. It can be seen from Figs. 3 and 4 that there are certain peaks that do not have arrows above them. The heights of the peaks without arrows are close but not equal to T_c. It is interesting to note that if the arrows of seven generations (Fig. 4) are placed on the transmissivity plot of the six generations (Fig. 3), then, except for the 12th, 15th and 24th peaks (counted from the left), all the peaks become associated with arrows above them. This can be explained by the fact that one generation before becoming a true identity matrix, the transfer matrix for the respective β often has a diagonal form close to the identity matrix. Thus almost all the peaks of the transmissivity plot are due to the fact that the trace of the transfer matrices becomes 1 at the corresponding values of β. This feature is common to all generations.

It is to be noted that if a new generation is added, the number of values of β that makes the trace of the transfer matrix equal to 1 becomes double of the number of such
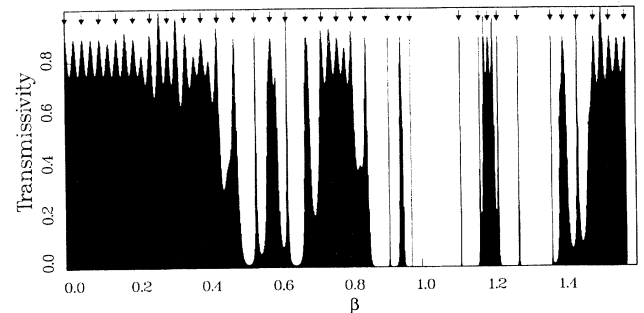

FIG. 4. Same as Fig. 3 for seven generations.

values of β for all the previous generations. This is shown in Fig. 5. In Fig. 5, the contributions to the list of values of β due to different generations are presented as vertical lines of different heights. It is seen that the values of β fall into groups. This grouping phenomenon can again be explained by superposing the set of initial conditions on the basin of attraction of Fig. 1. Initial conditions can be easily calculated for the transfer matrices of Eq. (27). We get

$$\bar{x}_0 = x_0 = \cos\beta, \quad y_0 = x_1 = 1 - C \sin^2\beta,$$

$$y_1 = 1 - C \sin^2 2\beta,$$

where

$$C = 1 + \frac{1}{2}\left(\frac{n_A}{n_B} + \frac{n_B}{n_A}\right).$$

Evidently, $C > 2$ for a nonperiodic system: $U_1 = -2C(C-2)\sin^4\beta$. One can easily eliminate β from these expressions. The set of initial values of the TM map is then the parabolic segment:

$$y_1 = \frac{1}{C}[4x_1^2 + 4(C-2)x_1 + 4-3C]; \quad 1-C < x_1 < 1.$$

Particularly, $\beta = 0$ corresponds to the initial point $(1,1)$. That explains the regular form of the transmissivity in Figs. 3 and 4 reminiscent of what we called the "Bloch-like" bands arising in the excitation spectra around such periodic orbits of the trace map as the $(1,1)$ point in this case. The value $\beta = \pi/2$ corresponds to the point $(1-C,1)$ also on the $y=1$ line. As β would increase further on, the initial point would move as a pendulum on the above parabola, explaining thus the periodic character of the transmissivity as the function of β.

Evidently, the special values of β corresponding to the constant peak heights of the transmissivity as described above, correspond to the intersections of the parabolic segment of the initial values of the TM map with the subset of the basin of attraction of the point $(1,1)$ of Fig. 1 that contains only the given number of generations of
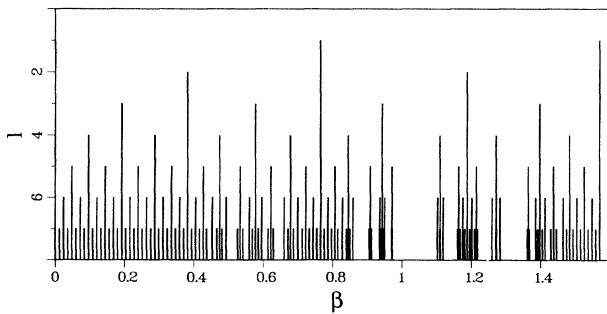

FIG. 5. Plot of l as a function of β. Here the values of β are such that $x_{l+2} = 1$ and the corresponding transfer matrix is an identity matrix. It can be seen that every new generation doubles the number of all previous β values. Some self-similarity in the plot is also noticeable.

the predecessors of the $(1,1)$ point. For six generations of the predecessors this is visualized in Fig. 6(a) where one can easily count the 33 interactions corresponding to the 33 values of β marked in Fig. 4. Some self-similarities in the cluster of β values are also evident from Figs. 5 and 6(b).

X. DIAMAGNETISM IN SUPERCONDUCTIVE WIRE NETWORKS AND JOSEPHSON-JUNCTION ARRAYS: THE THUE-MORSE CIRCUIT

Ordered sets of superconducting elements (wires, Josephson tunnel junctions, or proximity effect junctions) have been produced by using electron lithography and other techniques and a large number of experiments[36] have studied flux quantization in these two-dimensional
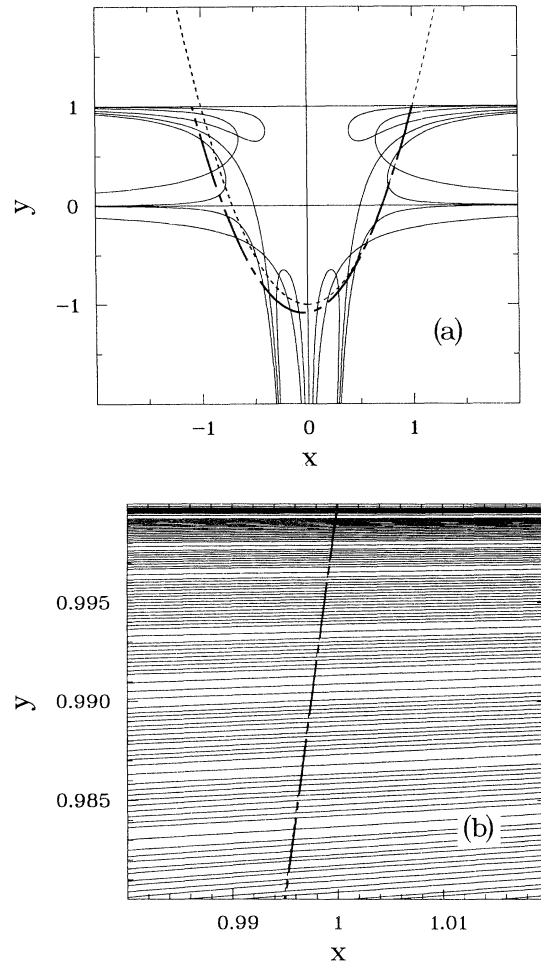

FIG. 6. Same as Fig. 1. The bold long and short dashed line represents the set of initial points (x_1, y_1) of the TM map corresponding to light transmission through multilayer medium with $n_A = 2$ and $n_B = 3$. 6 (a) and 13 (b) generations of the predecessors of the $(1,1)$ point are plotted. In (b) — the immediate vicinity of the $(1,1)$ point — the segment of the initial point parabola shown, corresponds to $\beta \in (0, 0.0025)$.

(2D) systems with an emphasis in periodic arrays. However, several groups have recently performed experiments with superconducting *ordered nonperiodic* structures with either fractal or quasicrystalline[37] geometry.

It is the purpose of this section to study the frustration induced on 2D Thue-Morse networks by an applied magnetic field and its effect on their superconducting diamagnetic properties. In particular, we calculate the associated superconducting-normal phase boundary, $T_c(H)$. In these systems, a continuous variation of the applied magnetic field allows the unique possibility for a fine tuning of the geometry-induced frustration. Note that the concept of frustration arises naturally in physical systems with competing interactions (or constraints). The lattices considered here have two types of elementary plaquettes: one denoted by l (for large) and the other denoted by s (for small). Also, the ratio of the elementary plaquette areas is equal to an irrational number (which we will arbitrarily choose to be τ, the golden mean) for all the lattices considered here. This geometric constraint implies that the magnetic flux cannot satisfy quantization in all the plaquettes simultaneously. We have considered[38-40] the linearized Ginzburg-Landau equations (for the superconducting networks) and the linearized mean-field approximation to the frustrated XY Hamiltonian (for the Josephson-junction array).

A. Josephson-junction arrays

Let us now consider a Josephson-junction array in an externally applied magnetic field. The Hamiltonian for such a system is given by

$$\mathcal{H} = - \sum_{\langle \alpha,\beta \rangle} J_{\alpha\beta} \cos(\varphi_\alpha - \varphi_\beta - A_{\alpha\beta}), \tag{28}$$

where φ_α is the phase of the superconducting order parameter $\Delta_\alpha = |\Delta_\alpha| e^{i\varphi_\alpha}$, $\langle \alpha,\beta \rangle$ denotes all pairs of nearest neighbors, $A_{\alpha\beta} = \frac{2\pi}{\Phi_0} \int_\alpha^\beta \mathbf{A} \cdot d\mathbf{l}$ is the circulation of the vector potential $\mathbf{A}$ along the bond linking α and β, and $\Phi_0 = ch/2e$ the elementary flux quantum. Even for regular periodic lattices, this Hamiltonian is very difficult to analyze in the presence of frustration. We will, therefore, solve it in the mean-field approximation.[40] The order parameter to be used is the canonical average of the phase factor, i.e.,

$$\eta_\alpha = \langle e^{i\varphi_\alpha} \rangle = \frac{1}{Z} \int \cdots \int d\varphi_1 \cdots d\varphi_N \, e^{i\varphi_\alpha} e^{-\mathcal{H}/k_B T}, \tag{29}$$

where Z is the partition function for N superconducting grains. Carrying out the complete calculation gives a set of N coupled nonlinear equations, for the N unknown complex phase order parameters η_α. For the particular case when T is near T_c, the phase variables are small, and so, therefore, are the expectation values. For this case, we can obtain the linearized mean-field equation

$$-\frac{1}{2k_B T} \sum_\beta \eta_\beta \, e^{iA_{\alpha\beta}} J_{\alpha\beta} = \eta_\alpha, \tag{30}$$

which is essentially a tight-binding Schrödinger equation for an electron of charge $2e$ hopping on an N site lattice immersed in an external magnetic field. $J_{\alpha\beta}$ is the analog of the hopping transition amplitude, the order parameter η_α is the complex wave function at the αth site, and $(k_B T)^{-1}$ is the energy eigenvalue. T_c is the highest value of T for which Eq. (30) has a nontrivial solution, i.e., it maps onto the band edge of the tight-binding Schrödinger equation.

B. Superconducting micronetworks

In order to compute the upper critical field of a superconducting micronetwork near the second-order phase boundary, in the context of mean-field theory, we need to solve the linearized Ginzburg-Landau equation. It has been shown that this approach leads in general to an eigenvalue problem, which is best expressed in terms of the order parameter values at the nodes. If node α is linked to n nodes via strands of length $L_{\alpha\beta}$ ($\beta = 1, \ldots, n$), the basic equation at node α is

$$\sum_{\beta=1}^{n} \Delta_\beta \, e^{iA_{\alpha\beta}} / \sin\left(\frac{L_{\alpha\beta}}{\xi_s}\right) = -\Delta_\alpha \sum_{\beta=1}^{n} \cot\left(\frac{L_{\alpha\beta}}{\xi_s}\right), \tag{31}$$

where Δ_β is the value of the order parameter at node β, and ξ_s the coherence length. Also, $\xi_s = \xi_0(T_{co}/\delta T)^{1/2}$ where $\delta T = T_{co} - T$. Thus, the superconducting state must satisfy $\delta T > T_{co}(\xi_s/\xi_0)^2$. For a lattice where $L_{\alpha\beta} \equiv L$ is the same for all links (e.g., square, triangular and Penrose networks), Eq. (31) reduces to that of a Landau-level structure of a free-electron gas in the same geometry, i.e., a tight-binding Schrödinger equation. In summary, in the context of mean-field theory, the variation of the highest eigenvalue as a function of the flux per plaquette [either small (s) Φ_s, or large (l) Φ_l] determines the effect of the frustration on the superconducting transition temperature.

If the array lies in the xy plane, and a magnetic field $\mathbf{B}$ is applied perpendicular to the array, then with our choice of gauge being $\mathbf{A} = Bx\hat{y}$, the phase $A_{\alpha\beta}$ can be written as $A_{\alpha\beta} = \frac{2\pi}{\Phi_0} B(y_\beta - y_\alpha)(x_\alpha + x_\beta)/2$, where x_α and y_α are the x and y coordinates of the center of grain α.

C. Strip-type Thue-Morse networks

In this section we compute $T_c(\Phi)$ for 2D Thue-Morse superconducting networks that are periodic in one direction. More specifically, we assume the networks to have a structure of a rectangular net with a uniform lattice spacing in the y direction and a variable spacing in the x direction (strip-type geometries). The mean-field equations (31) for a wire network can be reduced to a one-dimensional form:

$$-\frac{l^2}{2\xi^2}\,\phi_n \;=\; \left[\,2\cos(Blx_n + q) \;-\; \left(2 + \frac{l}{l_n} + \frac{l}{l_{n+1}}\right)\right]\alpha_n^{-1}\,\phi_n \;+\; \frac{l}{l_{n+1}}\,(\alpha_n\alpha_{n+1})^{-\frac{1}{2}}\,\phi_{n+1} \;+\; \frac{l}{l_n}\,(\alpha_n\alpha_{n-1})^{-\frac{1}{2}}\,\phi_{n-1},$$

where $\alpha_n = 2 + (l_n + l_{n+1})/l$, $l_n = x_n - x_{n-1}$, and x_n is the x coordinate of the lattice point (n, m). In the derivation of the above equations we have taken the gauge $\mathbf{A} = (0, Bx)$ and written ϕ_{nm} as $\phi_n\,e^{iqm}$. At this stage, we would like to remind the reader that we have taken $2\pi/\Phi_0$ as the unit of the magnetic field B, where Φ_0 is the flux quantum. In a similar fashion, the mean-field equation (30) for a Josephson-junction array can be reduced to a one-dimensional form:

$$2kT\,\phi_n \;=\; J_n^x\,2\cos(Blx_n + q)\,\phi_n$$
$$+\,J_{n+1}^y\,\phi_{n+1} \;+\; J_n^y\,\phi_{n-1},$$

where the J's are the coupling constants.

The two equations above, which have been derived from the mean-field equations (30) and (31), are formally identical. By numerically solving either one of them we obtain the transition temperature of a Thue-Morse superconducting circuit. The changes in the critical temperature when the system changes from a two-ladder network to a Thue-Morse circuit can be followed in Fig. 7. All the ladders consist of 500 equally spaced wires along the vertical direction, and an aperiodic sequence of small and large distances between wires in the horizontal direction. This, of course, creates an aperiodic sequence of large and small cells along the horizontal direction. The bottom curve, Fig. 7(a), refers to a two-ladder (i.e., it has three nonequally spaced vertical wires) network. It has a very smooth superconducting-normal phase boundary. Figure 7(b) corresponds to a network with four TM-ordered cells in the horizontal direction and 500 equally spaced wires along the vertical direction. The local maxima and minima of the corresponding $T_c(0) - T_c(\Phi)$ curve tend, in general, to be slightly more peaked (cusplike). Figure 7(c) corresponds to a circuit with eight TM-ordered cells. The corresponding reduced critical temperature starts developing a fine structure that is sensitive to long-range ordering (many-cells effect) stemming from the particular ordering of the TM sequence. This results suggest that a few-cells effect is responsible for the overall features including the quadratic extrema, while the cusplike behavior and the fine structure is due to the collective effect of many cells. By increasing the number of aperiodically ordered cells, only the fine structure of the phase boundary changes. The precise form of this very fine structure is sensitive to the TM ordering, since different sequences[38] produce different fine-structure profiles for the reduced critical temperature.

XI. SUMMARY

We have studied a large variety of physical properties of the Thue-Morse chain and its generalizations.

The fundamental question raised refers to the effect of the Thue-Morse ordering on the behavior of electrons, spins, phonons, electromagnetic waves, and superconducting order parameters. Since different definitions for the structure factor have been used by different authors, we have discussed them and, for several cases, derived the fundamental property that refers to the absence of spectral δ-function peaks. Subsequently, we presented a simple derivation of an expression for the location and

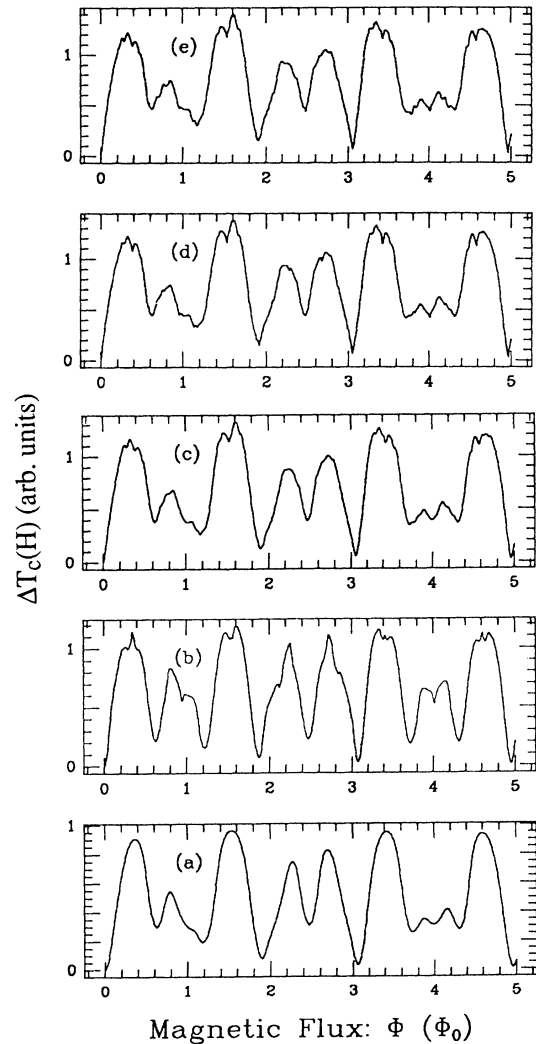Magnetic Flux: Φ (Φ_0)

FIG. 7. Superconducting-normal phase boundary for lattices with strip-type geometry. The quantity along the vertical axis is the reduced critical temperature, defined by $T_c(0) - T_c(\Phi)$. The quantity along the horizontal axis is the magnetic flux Φ. The number of cells along the vertical (periodic) direction is equal to 500. The number of cells (either large or small, Thue-Morse ordered) along the horizontal (aperiodic) direction is equal to successive powers of two: (a) 2, (b) 4, (c) 8, (d) 16, and (e) 32.

relative size of the spectral gaps. After this preliminary discussion of several basic features of the TM sequence, we focused on a detailed and systematic study of its electronic properties by using a trace-map approach expressed in terms of Chebyshev polynomials of the first and second kind. We derived the trace map for a generalized Thue-Morse sequence, which is *two-dimensional*, and proved it to be *area nonpreserving*. As a particular case, we obtained the simple tracemap for the original TM chain. The geometrical significance of the generalized map and its attractor has been discussed and illustrated. Furthermore, we can predict the structure of the spectra *without* going through the iterations of the TM trace map. We have illustrated the power of this method by considering two systems: the quantum Ising model in a transverse magnetic field and a diagonal electron hopping problem. Moreover, we analyzed and computed (i) the transmission coefficient for electromagnetic waves propagating through a TM multilayer and (ii) the aperiodic critical temperature obtained when varying the flux applied perpendicularly to a TM-ordered superconducting wire network or Josephson-junction array.

ACKNOWLEDGMENTS

*Current address: The Institute of Physical and Chemical Research (RIKEN), Hirosawa 2-1, Wako-shi, Saitama 351-01, Japan.

[1] R. Merlin, K. Bajema, R. Clarke, F. Juang, and P. K. Battacharya, Phys. Rev. Lett. **55**, 1768 (1985).

[2] R. Merlin, K. Bajema, J. Nagle, and K. Ploog, J. Phys. (Paris) Colloq. **48**, C5-503 (1987).

[3] Y. Duplain, T. Kamae, and M. Mendes-France, Arch. Mater. Mech. Anal. **34**, 2 (1986).

[4] F. Axel and J. Peyrière, C.R. Acad. Sci. Ser. II (France) **306**, 179 (1986).

[5] F. Axel, J.P. Allouche, M. Kleman, M. Mendes-France, and J. Peyrière, J. Phys. (Paris) Colloq. **47**, C3-181 (1986).

[6] S. Tamura and F. Nori, Phys. Rev. B **40**, 9790 (1989).

[7] M. Doria, F. Nori, and I. Satija, Phys. Rev. B **39**, 6802 (1989).

[8] R. Riklund, M. Severin, and Y. Liu, Int. J. Mod. Phys. B **1**, 121(1987).

[9] Z. Cheng, R. Savit, and R. Merlin, Phys. Rev. B **37**, 4375 (1988).

[10] J.M. Luck, Phys. Rev. B **39**, 5834 (1989).

[11] M. Kolář and M.K. Ali, Phys. Rev. B **41**, 7108 (1990).

[12] M. Kolář and M.K. Ali, Phys. Rev. A **39**, 6538 (1989).

[13] C.A. Tracy, J. Phys. A **21**, L603 (1988).

[14] V.G. Benza, M. Kolář, and M.K. Ali, Phys. Rev. B **41**, 9578 (1990).

[15] F. Nori and J. Rodriguez, Phys. Rev. B **34**, 2207 (1986); Q. Niu and F. Nori, Phys. Rev. Lett. **57**, 2057 (1986).

[16] M. Kohmoto, B. Sutherland, and C. Tang, Phys. Rev. B **35**, 1024 (1986); J.P. Lu, T. Odagaki, and J.L. Birman, *ibid.* **33**, 4809 (1986).

[17] G. Gumbs and M.K. Ali, Phys. Rev. Lett. **60**, 1081 (1988); J. Phys. A **21**, L517 (1988); Phys. Rev. B **38**, 7091 (1988).

[18] A. Thue, Norske Vididensk. Selsk. Skr. I. **7**, 1 (1906); **1**, 1 (1912).

[19] M. Morse, Trans. Am. Math. Soc. **22**, 84 (1921); Am. J. Math. **43**, 35 (1921).

[20] M. Keane, Z. Wahrsch. Gebiete **10**, 335 (1968).

[21] A. Cobham, Math. Syst. Theory **3**, 186 (1969); **6**, 164 (1972).

[22] G.T. Herman and G. Rozenberg, *Developmental Systems and Languages* (North-Holland, Amsterdam, 1975).

[23] G. Christol, T. Kamae, M. Mendes-France, and G. Rauzy, Bull. Soc. Math. (France) **108**, 401 (1980).

[24] F.M. Dekking, J. Combinatorial Theory **27A**, 292 (1976).

[25] E. Bombieri and J.E. Taylor, J. Phys. (Paris) Colloq. **47**, C3-19 (1986).

[26] C. Godrèche, J.M. Luck, and F. Vallet, J. Phys. A **20**, 4483 (1987).

[27] S. Aubry, C. Godrèche, and J.M. Luck, Europhys. Lett. **4**, 639 (1987).

[28] S. Aubry, C. Godrèche, and J.M. Luck, J. Stat. Phys. **51**, 1033 (1988).

[29] M. Queffèlec, *Substitutions, Dynamical Systems, Spectral Analysis*, Vol. 1294 of *Lecture Notes in Mathematics* (Springer, Berlin, 1987).

[30] J.P. Allouche and J. Peyrière, C.R. Acad. Sci. (France) **302**, 1135 (1986).

[31] M. Kolář and M.K. Ali, Phys. Rev. B **39**, 426 (1989); J. Phys.: Condens. Matter **1**, 823 (1989).

[32] B. Sutherland, Phys. Rev. Lett. **57**, 770 (1986).

[33] V.G. Benza, Europhys. Lett. **8**, 321 (1989).

[34] M. Kohmoto, B. Sutherland, and K. Iguchi, Phys. Rev. Lett. **58**, 2436 (1987); G. Gumbs and M. K. Ali, J. Phys. A **22**, 951 (1989).

[35] M. Born and E. Wolf, *Principles of Optics* (Pergamon, New York, 1980), Chap. 1.

[36] For recent reviews, see B. Pannetier, J. Chaussy, and R. Rammal, Jpn. J. Appl. Phys. **26**, Suppl. 26-3, 1994 (1987); P. Martinoli, *ibid.* **26**, Suppl. 26-3, 1989 (1987).

[37] A. Behrooz et al., Phys. Rev. Lett. **57**, 368 (1986); Phys. Rev. B **35**, 8396 (1987); K. Springer and D. Van Harlingen, *ibid.* **36**, 7273 (1987); Y.Y. Wang et al., Jpn. J. Appl. Phys. **26**, Suppl. 26-3, 1415 (1987).

[38] Q. Niu and F. Nori, Phys. Rev. B **39**, 2134 (1989).

[39] F. Nori, Q. Niu, E. Fradkin, and S.J. Chang, Phys. Rev. B **36**, 8338 (1987); F. Nori and Q. Niu, *ibid.* **37**, 2360 (1988); P. Santhanam, C.C. Chi, W.W. Molzen, *ibid.* **37**, 2364 (1988); F. Nori and Q. Niu, Physica B **152**, 105 (1988).

[40] W.Y. Shih and D. Stroud, Phys. Rev. B **28**, 6575 (1983); **30**, 6774 (1984); **32**, 158 (1985).